Pancreatic Stiffness Quantified with MR Elastography: Relationship to Postoperative Pancreatic Fistula after Pancreaticoenteric Anastomosis

Yu Shi, MD • Ying Liu, MBBS • Feng Gao, MS • Yanqing Liu, MBBS • Shengzhen Tao, MS • Yue Li, MS • Kevin J. Glaser, PhD • Richard L. Ehman, MD • Qiyong Guo, MD

From the Departments of Radiology (Y.S., Ying Liu, Yanqing Liu, Q.G.), Pancreato-thyroidic Surgery (F.G.), and Pathology (Yue Li), Shengjing Hospital, China Medical University, No. 36 Sanhao St, Heping District, Shenyang 110004, P.R. China; and Department of Radiology, Mayo Clinic, Rochester, Minn (S.T., K.J.G., R.L.E.).
Received February 23, 2017; revision requested April 18; revision received January 14, 2018; final version accepted January 16, 2018. **Address correspondence to** Q.G. (e-mail: *guoqiyongcmu@163.com*).

Supported by the National Natural Science Foundation of China (Y.S.: grants 81771802, 81401376; Q.G: grants 81771893, 81471718). R.L.E. supported by National Institutes of Health (grant EB001981).

Conflicts of interest are listed at the end of this article.

Radiology 2018; 288:476–484 • https://doi.org/10.1148/radiol.2018170450 • Content code: GI

Purpose: To describe the relationship between conventional magnetic resonance (MR) imaging parameters and MR elastography of the pancreas in association with pancreatic histologic features and occurrence of postoperative pancreatic fistula (POPF).

Materials and Methods: Patients who underwent preoperative MR imaging (MR elastography and diffusion-, T1-, and T2-weighted imaging) followed by pancreatectomy with pancreaticoenteric anastomosis were included. The relationships between preoperative MR imaging parameters, demographic data, and intraoperative factors with POPF risk were analyzed with logistic regression analyses. The correlation of MR imaging parameters with histologic characteristics was evaluated with multivariate regression analysis.

Results: A total of 112 patients (64 men, 48 women; median age, 58 years) were evaluated. Forty-two patients (37.5%) developed POPF and 20 (17.9%) developed high-grade POPF (grades B and C). Lower pancreatic stiffness (≤1.43 kPa; odds ratio [OR], 9.196; 95% confidence interval [CI]: 1.92, 43.98), nondilated main pancreatic duct (MPD) diameter (<3 mm; OR, 7.298; 95% CI: 1.51, 35.34), and larger stump area (≥211 mm^2; OR, 9.210; 95% CI: 1.53, 55.26) were risk factors for POPF. Lower pancreatic stiffness (≤1.27 kPa; OR, 8.389; 95% CI: 1.88, 37.41) was the only independent predictor of high-grade POPF. Log-transformed pancreatic stiffness was independently associated with fibrosis (β = 0.060; 95% CI: 0.052, 0.068), acinar atrophy (β = 0.015; 95% CI: 0.003, 0.028), and lipomatosis (β = −0.016; 95% CI: −0.026, −0.006).

Conclusion: Preoperative MR assessment of pancreatic stiffness, MPD diameter, and stump area are important predictors of POPF.

Online supplemental material is available for this article.

Postoperative pancreatic fistula (POPF), which can potentially lead to catastrophic abscess and hemorrhage, is one of the most serious complications of pancreatectomy (1) and remains the leading risk factor for postoperative morbidity and mortality (2,3).

Several preoperative imaging indicators of POPF risk have been identified (4–8), including morphologic features of the pancreatic stump (eg, thickness, area, main pancreatic duct [MPD] diameter), signal intensity at T1-weighted imaging, apparent diffusion coefficient (ADC), and fat fraction. These parameters are used to evaluate the morphologic characteristics or to establish a correlation with histologic changes (eg, fibrosis) of the pancreatic stump (9,10). However, none of these parameters can be used to directly assess pancreatic texture or stiffness. Magnetic resonance (MR) elastography was developed as a technique to measure tissue stiffness (11). Following the development of a three-dimensional wave field inversion algorithm based on acquisition of spin-echo echo-planar images, MR elastography has been successfully applied in organs with complex geometry, including the brain, lung, and pancreas (12–16). Moreover, 40-Hz vibration with a pancreas-tailored soft driver provided robust estimates of tissue shear stiffness in both healthy and diseased pancreas and provided a better wave pattern and higher amplitude of motion than did imaging at 60 Hz (12,15,17). In our study, we hypothesized that the morphologic and mechanical qualities of the pancreatic stump measured with preoperative MR imaging could serve as accurate markers for predicting POPF.

Thus, the purpose of our study was to describe the performance of several MR parameters, including morphologic features, pancreatic stiffness, ADC, and signal intensity at T1-weighted imaging of the pancreatic stump, for predicting POPF and to study the histologic changes underlying these parameters.

Materials and Methods

Patients

We retrospectively reviewed a single-center, prospectively maintained database with approval from the local institutional review board. We evaluated patient studies obtained between December 2013 and August

Abbreviations

ADC = apparent diffusion coefficient, CI = confidence interval, MPD = main pancreatic duct, OR = odds ratio, POPF = postoperative pancreatic fistula

Summary:

Quantitative preoperative MR assessments of mechanical and morphologic characteristics of the pancreatic stump are strongly predictive of pancreaticoenteric anastomotic fistula. Lower pancreatic stiffness was associated with relatively less pancreatic fibrosis, higher grade of acinar atrophy, and lipomatosis.

Implications for Patient Care

- Pancreatic stiffness showed a positive association with pancreatic fibrosis and acinar atrophy but an inverse association with pancreatic lipomatosis.
- Lower pancreatic stiffness at MR elastography was the strongest risk factor for postoperative pancreatic fistula (POPF) in multivariate analysis that assessed several MR parameters, patient characteristics, and intraoperative factors.
- Preoperative MR quantification of pancreatic stiffness may serve as an imaging biomarker for POPF risk in patients undergoing pancreatectomy with pancreaticoenteric anastomosis and could supersede risk prediction based on subjective assessment by surgical palpation.

2017. MR elastography was added to the routine pancreatic MR imaging protocol in patients who gave written informed consent to accept the inclusion of MR elastography into his or her clinical pancreatic MR protocol. The 167 consecutive patients who underwent both pancreatectomy and preoperative pancreatic MR imaging in the local hospital were included initially. However, 55 patients were excluded, 17 for technical failure of MR elastography (detailed in Appendix E1 [online], determined both at the time of the original MR imaging and upon retrospective review), 22 because surgery was performed without pancreaticoenteric anastomosis, and 16 for inadequate specimens (Fig 1). Thus, we included 112 patients (median age, 58.0 years; range, 21–76 years): 64 men (median age, 60.0 years; range, 21–76 years) and 48 women (median age, 54.0 years; range, 31–74 years). These patients underwent pancreatectomy for the following indications: pancreatic ductal adenocarcinoma (n = 49), chronic pancreatitis (n = 20), pancreatic neuroendocrine tumor (n = 7), intraductal papillary mucinous neoplasm (n = 5), solid pseudopapillary tumor (n = 7), serous cystadenoma (n = 3), mucinous cystadenoma (n = 1), common bile duct cancer (n = 4), cancer of the ampulla of Vater (n = 15), and duodenal carcinoma (n = 1). Patient characteristics, imaging features, intraoperative factors (anastomosis, surgery time, blood loss, pancreatic texture determined with surgeon's palpation, stump mobilization, and MPD diameter assessed intraoperatively), and postoperative histologic features in POPF and non-POPF groups are shown in Table 1.

The Mayo Clinic and two authors (K.J.G. and R.L.E.) have intellectual property rights and financial interest in MR elastography. The authors without conflict of interest (Y.S. and Q.G.) controlled the data for the study.

Image Acquisition

All patients were instructed to fast completely for at least 8 hours before the examination to avoid possible alteration of pancreatic perfusion and compression by a full stomach. MR examinations were performed by using a 3.0-T MR system (Signa HDX; GE Healthcare, Milwaukee, Wis) with an eight-channel phased-array body coil. Our MR protocol included the following pulse sequences (detailed imaging parameters are summarized in Table E1 [online]): *(a)* axial T1- and T2-weighted imaging (with and without fat suppression), *(b)* MR elastography, *(c)* quick breath-hold diffusion-weighted imaging acquisition with b values of 0 and 800 sec/mm^2 (four signals acquired, acquisition time included two 22-second breath holds), and *(d)* coronal images with fast imaging obtained with steady-state acquisition. The total acquisition time was approximately 15–20 minutes. MR elastography was performed by using 40-Hz vibrations and a 32-section spin-echo echo-planar imaging pulse sequence that covered the entire pancreas to obtain volumetric vector displacement for imaging the propagating shear waves (12,15,17,18). See Appendix E1 (online) and Figure E1 (online) for details of MR elastographic acquisitions, failures, and verification of wave propagation.

Image Analysis

The feasibility of MR elastography was assessed on the basis of another separate prospective study involving 40 healthy volunteers. The reproducibility of MR elastographic acquisition was assessed in 20 of 40 volunteers and in 10 of the 112 patients by two readers (a primary reader, Y.S., with 5 years of experience interpreting MR elastograms, and a secondary reader, Ying Liu, with 3 years of MR elastography experience), as detailed in Appendix E1 (online). After the feasibility and reproducibility of MR elastography were established, only the stiffness values from the primary reader were further used. To measure stiffness, regions of interest were drawn on the magnitude images to outline the pancreatic stump; they were transferred automatically from the magnitude image to the wave images and elastograms to obtain tissue stiffness values in kilopascals. Care was taken to ensure that magnitude images had sufficient illumination and had no noise, flow, or motion artifacts affecting the pancreas. Both the wave images and the local frequency estimation confidence map were checked to verify wave propagation within each region of interest of the pancreas. Invalid wave data were defined as both wave images and local frequency estimation confidence maps that showed invalid results (detailed in Appendix E1 and Fig E1 [online]).

Additional measurements were obtained by the primary reader, who was unaware of the clinical and histopathologic findings except for tumor location and surgical procedure. Regions of interest were drawn on elastograms (mean area ± standard deviation, 322.6 mm^2 ± 185.7), T1-weighted images (mean area, 221.9 mm^2 ± 144.2), and ADC maps of the pancreatic parenchyma (mean area, 234.6 mm^2 ± 166.4) near the resection margin; masses, artifacts, boundaries, and visible pancreatic duct were avoided (Fig 2). All parameters were calculated by averaging the measurements from three sections (± one section) (19,20). To calculate the signal intensity ratio on T1-weighted images,

two round regions of interest (approximately 80–150 mm^2) were drawn in the bilateral paraspinal muscles. The diameter of the MPD and the width of the pancreatic stump were measured on the axial T2-weighted images. The thickness of the pancreatic stump was measured on the coronal images. The stump area was calculated by multiplying pancreatic thickness by pancreatic width. The pancreas-to-duct ratio was calculated by dividing pancreatic thickness by MPD diameter. The pancreatic volume was calculated by multiplying the estimated area of pancreatic tissue on each section by the interval between sections based on T1-weighted images. For all measurements, the regions of interest were kept constant among all MR images and carefully adjusted by the primary reader. An MPD diameter of less than 3 mm was considered normal, that is, nondilated. A body mass index of less than 25 kg/m^2 was considered normal.

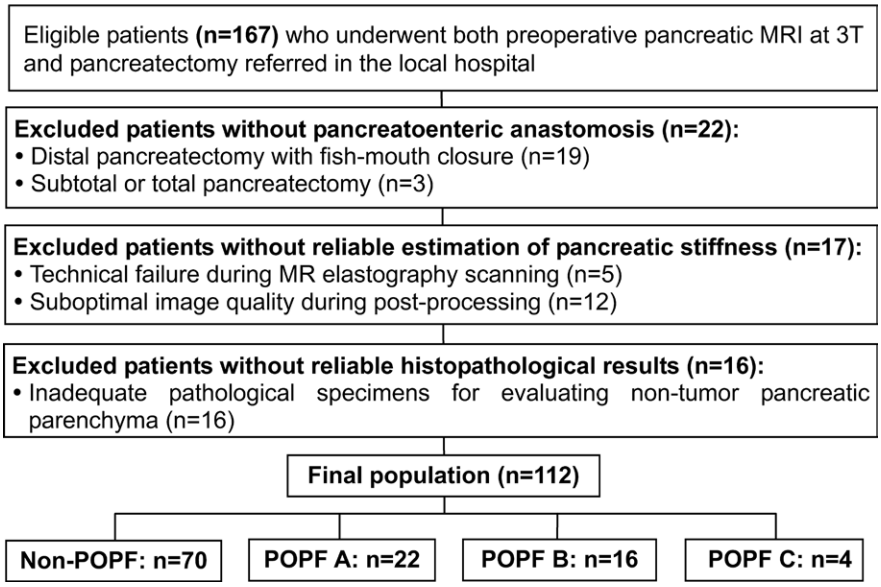

Figure 1: Flow chart illustrates patient selection process for study cohort. *POPF* = postoperative pancreatic fistula.

Clinical Data Collection

All surgeries were performed by a lead pancreatobiliary surgeon (F.G., with 18 years of experience in pancreatic surgery) and a dedicated surgical team. The lead surgeon and an assistant surgeon (with 10 years of experience in pancreatic surgery) assessed the firmness of the pancreatic stump, which was recorded as soft, medium, or hard, by intraoperative palpation (21). The MPD diameter, stump area, and mobilization of the pancreatic remnant (in millimeters) were also measured intraoperatively at the cut surface. The interval between MR imaging and pancreatectomy ranged from 1 to 21 days (median, 7 days). The clinical data collection is detailed in Appendix E1 (online). The criteria for POPF grades A, B, and C are summarized in Table E2 (online) (22).

Pathologic Evaluation

Histologic evaluation of the pancreatic surgical specimens was performed by two experienced pathologists who were blinded to the radiologic findings and clinical data (Yue Li and one nonauthor, with 12 and 17 years of experience in pancreatic pathology, respectively) in consensus. Pancreatic fibrosis at the resection margin was graded as F0, normal parenchyma with no fibrotic change; F1, mild fibrosis with thickening of periductal fibrous tissue; F2, moderate fibrosis with marked sclerosis of interlobular septa and no evidence of architectural change; and F3, severe fibrosis with architectural disruption (23). The severity of exocrine gland atrophy was classified according to the percentage of viable exocrine gland area as A0 (mild), 75%–100%; A1 (moderate), 25%–75%; and A2 (severe), 0%–25% (24). The degree of lipomatosis was graded as L0 (normal), 0%–10%; L1 (mild), 10%–20%; L2 (marked), 20%–30%; and L3 (severe), greater than 30% (4,9).

Statistical Analysis

Statistical analysis is detailed in Appendix E1 (online). To determine the accuracy of parameters for predicting POPF, nonparametric receiver operating characteristic curves were composed, and cutoffs were determined by maximizing the sum of sensitivity and specificity. Jackknife leave-one-out cross-validation was applied to all the obtained performance indexes to generate cross-validated parameters. A multivariate logistic regression model was used to determine the relative importance in predicting POPF and high-grade POPF, respectively, of risk factors selected because they appeared associated with POPF and/or high-grade POPF ($P < .10$), in either univariate logistic regression analysis or correlation analysis (Table 1). Strengths of associations were presented as odds ratios (ORs) with 95% confidence intervals (CIs). Stepwise multiple linear regression tests were conducted to study the association between histologic changes and the log-transformed pancreatic stiffness (normally distributed). Cross-validation of receiver operating characteristic analysis was performed with R software (R version 3.4.0; R Project for Statistical Computing). All other statistical analyses were performed by using SPSS software (version 16.0 J; IBM, Chicago, Ill).

Results

Correlation of Preoperative MR Imaging Parameters with Histologic Findings

Table 2 summarizes the distribution of MR imaging parameters stratified according to fibrosis stage (acinar atrophy and lipomatosis are summarized in Table E3 [online]). Pancreatic fibrosis showed a strong positive correlation with pancreatic stiffness ($r = 0.797$; $P < .001$), a weak positive correlation with MPD diameter ($r = 0.398$; $P < .001$), and a negative correlation with signal intensity ratio at T1-weighted imaging

Table 1: Univariate Analysis of Clinical Risk Factors for Postoperative Pancreatic Fistula

Parameter	No. of Patients or Median Value*			Correlation Coefficient†	
	All Patients	POPF	No POPF	POPF	High-Grade POPF
Patient characteristics					
Age (y)	58 (51–62)	58 (48–62)	59 (51–62)	−0.118 (.216)	−0.124 (.191)
Sex (M/F)	64/48	26/16	38/32	0.129 (.248)	0.086 (.444)
BMI (kg/m^2)	22.8 (20.5–24.3)	23.4 (21.0–24.7)	22.6 (20.5–24.7)	0.240 (.011)‡	0.167 (.078)‡
Diabetes mellitus (yes/no)	35/77	16/26	19/51	0.114 (.230)	0.083 (.386)
History of weight loss (yes/no)§	62/50	19/23	43/27	−0.158 (.097)‡	−0.044 (.648)
History of jaundice (yes/no)	41/71	18/24	23/47	0.100 (.292)	0.081 (.395)
History of smoking (yes/no)	66/46	23/19	43/27	−0.066 (.492)	−0.132 (.165)
Alcohol abuse (yes/no)	12/100	4/38	8/62	−0.109 (.253)	−0.111 (.243)
MR imaging parameters					
MPD diameter (mm)	3.3 (2.5–4.4)	2.9 (2.2–3.5)	3.5 (3.0–4.7)	−0.389 (<.001)‡	−0.273 (.004)‡
Stiffness at MR elastography (kPa)	1.34 (1.22–1.57)	1.24 (1.15–1.34)	1.49 (1.28–1.68)	−0.472 (<.001)‡	−0.422 (<.001)‡
SI ratio at T1-weighted imaging	1.44 (1.26–1.61)	1.59 (1.32–1.77)	1.37 (1.24–1.53)	0.114 (.233)	0.052 (.589)
ADC (×10^3 mm^2/sec)	1.39 (1.32–1.46)	1.38 (1.33–1.47)	1.41 (1.32–1.46)	−0.017 (.862)	−0.005 (.955)
Pancreatic thickness (mm)	15.5 (14.4–17.9)	17.5 (15.1–18.0)	15.1 (14.4–17.7)	0.160 (.092)‡	0.179 (.059)‡
P/D	4.02 (3.09–5.46)	5.09 (4.10–6.34)	3.73 (2.97–4.41)	0.410 (<.001)‡	0.336 (<.001)‡
Stump area (mm^2)	200 (169–277)	266 (199–287)	188 (168–271)	0.255 (.007)‡	0.304 (.001)‡
Remnant volume (cm^3)	20.3 (16.9–28.2)	26.3 (17.8–30.0)	19.3 (16.3–25.4)	0.238 (.011)‡	0.307 (.001)‡
Operative and intraoperative factors					
Anastomosis (end-to-side/duct-to-mucosa)	63/49	24/18	39/31	0.125 (.190)	0.110 (.246)
Operative time (min)	453 (352–514)	458 (354–534)	442 (325–492)	0.116 (.224)	0.130 (.170)
Blood loss (mL)	470 (338–528)	482 (355–596)	449 (328–509)	0.127 (.183)	0.123 (.198)
Pancreatic texture by surgeon's palpation					
Soft/medium/hard	47/53/12	24/18/0	23/35/12	−0.293 (.002)‡	−0.199 (.035)‡
Stump mobilization (mm)	35 (25–45)	35 (27–47)	33 (23–43)	0.181 (.057)‡	0.011 (.912)
MPD diameter (mm)	3.4 (2.5–4.7)	2.7 (2.1–3.4)	4.1 (3.1–5.2)	−0.379 (<.001)‡	−0.294 (.002)‡
Histopathologic features of pancreatic stump					
Fibrosis (F0/F1/F2/F3)	59/27/11/15	34/8/0/0	25/19/11/15	−0.552 (<.001)‡	−0.343 (<.001)‡
Acinar atrophy (A0/A1/A2)	56/45/11	29/13/0	27/32/11	−0.321 (.001)‡	−0.360 (<.001)‡
Lipomatosis (L0/L1/L2/L3)	62/33/14/3	19/15/6/2	43/18/8/1	0.159 (.100)	0.177 (.062)‡
Histopathologic features of mass					
PDAC or CP (yes/no)	69/43	20/22	49/21	−0.223 (.018)‡	−0.159 (.094)‡
Ampullary (yes/no)	15/97	6/36	9/61	0.020 (.832)	0.090 (.343)
Cholangiocellular (yes/no)	4/108	1/41	3/67	−0.050 (.603)	−0.036 (.707)
IPMN (yes/no)	5/107	2/40	3/67	0.050 (.603)	0.090 (.347)

Note.—ADC = apparent diffusion coefficient, BMI = body mass index, CP = chronic pancreatitis, IPMN = intraductal papillary mucinous neoplasm, MPD = main pancreatic duct, P/D = pancreas-to-duct ratio, PDAC = ductal pancreatic carcinoma, SI = signal intensity.
* Numbers in parentheses are the interquartile range.
† Numbers in parentheses are *P* values, which were calculated with the nonparametric Spearman correlation test.
‡ Statistically significant ($P < .10$).
§ Weight loss (≥3 kg over the previous 6 months) was assessed by patient interview before MR examination.

($r = -0.317$; $P = .001$) and pancreas-to-duct ratio ($r = -0.411$; $P < .001$). ADCs tended to decrease as fibrosis progressed but did not differ significantly ($r = -0.157$; $P = .098$). Having pancreatic ductal adenocarcinoma or chronic pancreatitis was positively correlated with both fibrosis ($r = 0.449$; $P < .001$) and pancreatic stiffness ($r = 0.543$; $P < .001$) and tended to be correlated with MPD size ($r = 0.168$; $P = .076$).

Multivariate regression analysis showed that log-transformed pancreatic stiffness was independently associated with pancreatic fibrosis (β = 0.060; 95% CI: 0.052, 0.068; $P < .001$), acinar atrophy (β = 0.015; 95% CI: 0.003, 0.028; $P = .018$), and lipomatosis (β = –0.016; 95% CI: –0.026, –0.006; $P = .001$). Approximately 73.7% of the total variability in pancreatic stiffness values could be explained by these three variables in this model (adjusted $R^2 = 0.737$, $P < .001$).

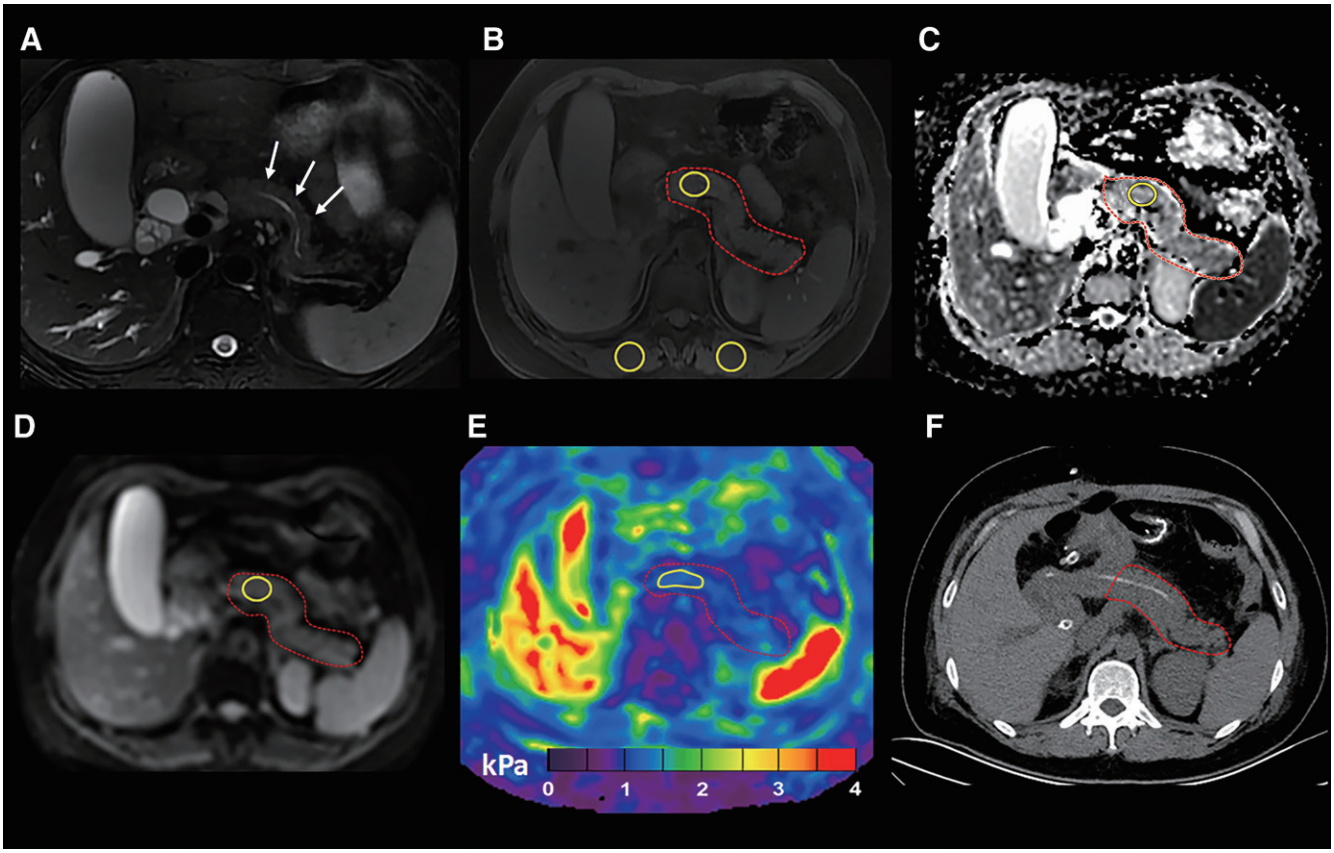

Figure 2: Preoperative MR images and postoperative CT scan in 47-year-old woman undergoing pancreaticoduodenectomy for pancreatic ductal adenocarcinoma. Regions of interest (in yellow) were placed near resection margin. Pancreatic parenchyma is outlined in red. Postoperative histologic assessment showed mild fibrosis (F1) of the pancreatic stump without pathologic acinar atrophy (A0) or lipomatosis (L0). *A*, T2-weighted image shows nondilated, 2-mm-diameter pancreatic duct (arrows). *B*, T1-weighted MR image shows oval regions of interest in pancreas and bilateral paraspinal muscles. Pancreas-to-muscle signal intensity ratio was 1.16. *C*, Apparent diffusion coefficient (ADC) map obtained at *b* value of 800 sec/mm^2 shows oval region of interest. Mean ADC was 1.38 mm^2/sec ± 0.22. *D*, Magnitude image shows oval region of interest in pancreas. *E*, Elastogram obtained in same cross-section coregistered with the magnitude image in *D*. Mean stiffness value was 1.22 kPa ± 0.68. *F*, Postoperative follow-up CT scan shows pancreaticojejunal anastomosis site. Figure E2 (online) and further clinical evaluation helped confirm grade A postoperative pancreatic fistula.

Table 2: Imaging Parameters Stratified according to Histologic Fibrosis Stage

Parameter	F0 (n = 59)	F1 (n = 27)	F2 (n = 11)	F3 (n = 15)	r*
Stiffness (kPa)	1.24 ± 0.13	1.42 ± 0.12	1.65 ± 0.08	1.94 ± 0.28	0.797 (<.001)†
SI ratio at T1-weighted imaging	1.48 ± 0.29	1.5 ± 0.3	1.35 ± 0.17	1.13 ± 0.28	−0.317 (.001)†
ADC (×10^3 mm^2/sec)	1.4 ± 0.11	1.46 ± 0.18	1.39 ± 0.06	1.32 ± 0.07	−0.157 (.098)
MPD diameter (mm)	3.01 ± 0.94	3.98 ± 1.55	3.71 ± 1.11	4.89 ± 2.36	0.398 (<.001)†
Thickness (mm)	16.26 ± 2.1	15.03 ± 2.53	16.46 ± 2.34	16.45 ± 1.7	−0.076 (.426)
Stump area (mm^2)	234.2 ± 59.8	190.3 ± 69.3	222.2 ± 78.7	232.4 ± 51.7	−0.159 (.095)
P/D	5.20 ± 1.68	3.77 ± 1.96	4.20 ± 1.28	3.41 ± 1.14	−0.411 (<.001)†
Remnant volume (cm^3)	23.1 ± 6.7	19.4 ± 7.5	22.3 ± 8.2	23.2 ± 5.7	−0.091 (.342)

Note.—Unless otherwise noted, data are means ± standard deviations. ADC = apparent diffusion coefficient, MPD = main pancreatic duct, P/D = pancreas-to-duct ratio, SI = signal intensity.
* r is the Spearman correlation coefficient obtained from the nonparametric Spearman correlation test. Numbers in parentheses are P values.
† Statistically significant ($P < .05$).

Performance of Parameters for Predicting POPF

The incidence rates of POPF and high-grade POPF were, respectively, 37.5% (42 of 112 patients) and 17.9% (20 of 112 patients) (Fig 2). Univariate analysis (Table 1) showed that the risk for POPF showed a significant correlation with preoperative parameters, including pancreatic stiffness, stump area, remnant volume, pancreas-to-duct ratio, MPD diameter, body mass index, weight loss, intraoperative pancreatic texture at

Table 3: Multivariate Analysis of Risk Factors for Postoperative Pancreatic Fistula

	POPF (n = 42)		High-grade POPF (n = 20)	
Parameter	Odds Ratio*	P Value	Odds Ratio*	P Value
Lower stiffness	9.196 (1.92, 43.98)†	.005†	8.389 (1.88, 37.41)†	.005†
Nondilated MPD	7.298 (1.51, 35.34)†	.014†	1.411 (0.25, 8.02)	.698
P/D	1.350 (0.30, 6.66)	.667	4.389 (0.63, 30.48)	.135
Stump area	9.210 (1.53, 55.26)†	.015†	2.300 (0.14, 8.15)	.561
Remnant volume	0.805 (0.15, 4.48)	.805	4.821 (0.34, 68.18)	.245
Normal BMI	0.685 (0.16, 2.83)	.601	0.303 (0.03, 3.00)	.307
No weight loss	2.485 (0.76, 8.18)	.134	1.149 (0.25, 5.27)	.858
Palpation	1.614 (0.42, 6.20)	.485	3.544 (0.73, 17.10)	.116
Stump mobilization	1.000 (0.96, 1.05)	.985	0.897 (0.19, 4.16)	.889
PDAC or CP	0.825 (0.18, 3.71)	.802	0.282 (0.04, 1.91)	.195

Note.—Multivariate analyses were performed by using a logistic regression model including all parameters with $P < .10$ in the univariate analysis (Table 1). BMI = body mass index, CP = chronic pancreatitis, MPD = main pancreatic duct, P/D = pancreas-to-duct ratio, PDAC = pancreatic ductal adenocarcinoma.
* Numbers in parentheses are 95% confidence intervals.
† Statistically significant ($P < .05$).

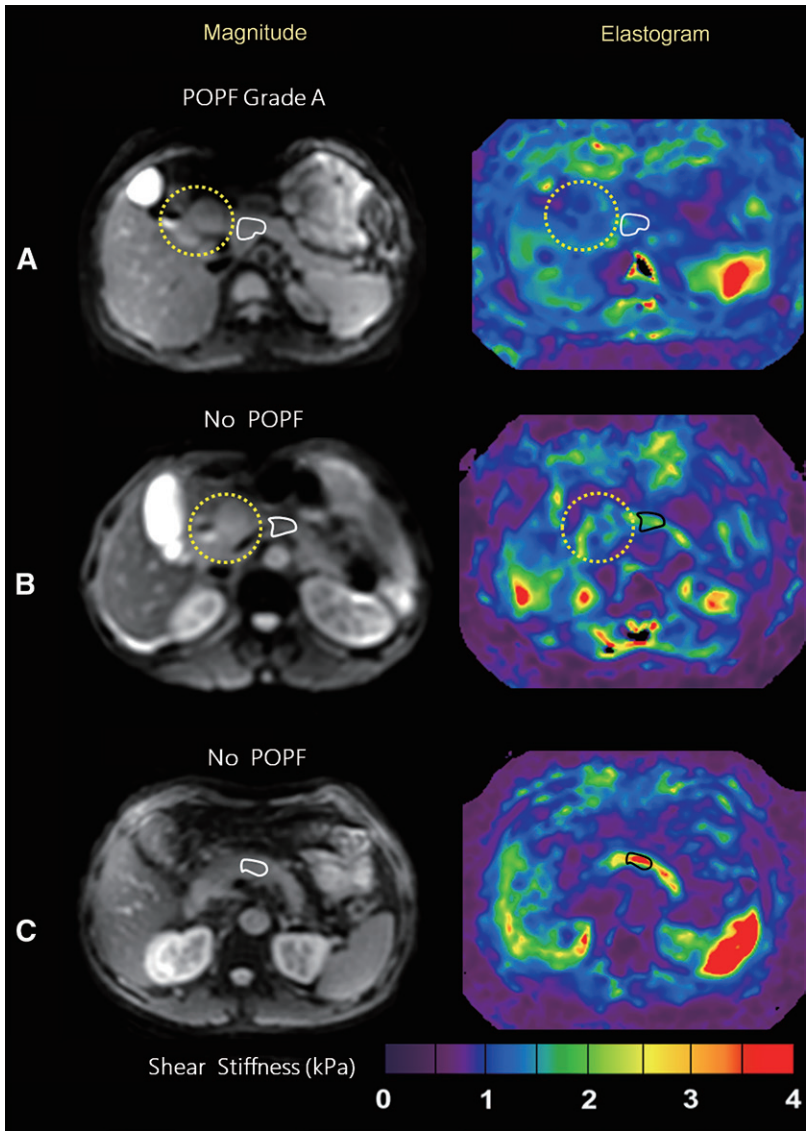

Figure 3: Axial MR magnitude images (left column) and MR elastograms (right column) from three cases: One case developed grade A postoperative pancreatic fistula (POPF) and two did not develop POPF. *A,* Images in 36-year-old woman who underwent pancreaticoduodenectomy for solid pseudopapillary neoplasm (yellow circle). Elastogram shows that mean stiffness value of pancreatic stump (white outline) was 1.19k Pa ± 0.32 with POPF grade A. *B,* Images in 64-year-old man who underwent pancreaticoduodenectomy for cystadenoma (yellow circle). Elastogram shows that mean stiffness value of pancreatic stump (black outline) was 1.89 kPa ± 0.31 without POPF. *C,* Images in a 55-year-old man who underwent pancreaticoduodenectomy for focal chronic pancreatitis (mass not shown). Elastogram shows that mean stiffness value of pancreatic stump (black outline) was 2.41kPa ± 0.43. All corresponding wave images are shown in Figure E1 (online).

palpation, stump mobilization, and diagnosis of either pancreatic ductal adenocarcinoma or chronic pancreatitis. On the basis of multivariate analysis (Table 3), lower pancreatic stiffness (≤1.43 kPa) (OR, 9.196 [95% CI: 1.92, 43.98]), nondilated MPD (OR, 9.210 [95% CI: 1.53, 55.26]), and larger stump area (≥211 mm^2) (OR, 7.298 [95% CI: 1.51, 35.34]) were independently associated with increased risk for POPF. Lower pancreatic stiffness was the only independent preoperative risk factor for high-grade POPF (OR, 8.389 [95% CI: 1.88, 37.41]).

Pancreatic stiffness (median, 1.49 kPa; interquartile range, 1.28–1.68 kPa) was significantly greater in patients without POPF than in those with grade A POPF (median, 1.32 kPa; interquartile range, 1.19–1.37 kPa) and high-grade POPF (median, 1.23 kPa; interquartile range, 1.12–1.24 kPa)

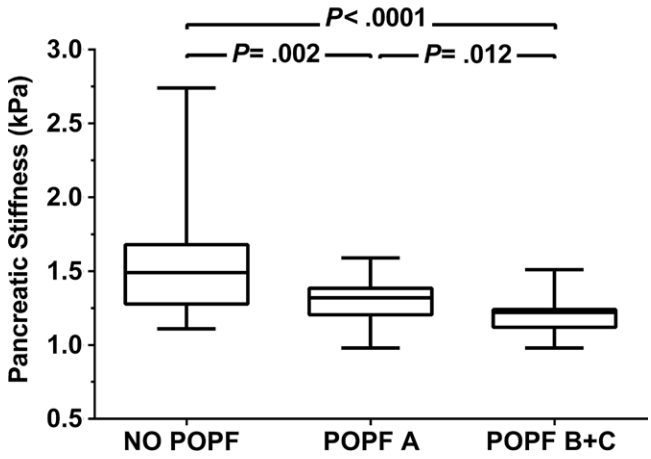

Figure 4: Box plots show pancreatic stiffness at MR elastography for patients without postoperative pancreatic fistula (POPF), with POPF grade A, and with POPF grades B and C. Boundaries of box indicate 25th and 75th percentiles, line within box indicates median, and whiskers indicate range. Horizontal brackets indicate significant differences in paired comparison by using Mann-Whitney *U* test with Bonferroni correction ($P < .017$ for all).

(Mann-Whitney *U* test, $P = .002$ and $P < .0001$, respectively), as shown in Figures 3 and 4. Raw and cross-validated estimates of diagnostic accuracy to predict POPF with both MR elastography and surgeon's palpation are reported in Tables 4 and 5, respectively. Both raw and cross-validated estimates show that MR elastography had higher accuracy than did palpation for predicting POPF (stiffness ≤1.43 kPa: 70.5% vs 63.4% for raw estimate [$P < .001$] and 67.9% vs 63.4% for cross-validated estimate [$P = .383$]) and high-grade POPF (stiffness ≤1.27 kPa: 73.2% vs 61.6% for both raw and cross-validated estimates [$P < .001$ for both]). When the cutoff for pancreatic stiffness was defined as greater than 1.59 kPa (1.51 kPa for high-grade POPF), the specificity reached 100%, with 100% negative predictive value. Stiffness still had significantly better sensitivity than did palpation for POPF ($P < .001$ for raw data and $P = .003$ for cross-validated data) and for high-grade POPF ($P = .003$ for raw data and $P = .006$ for cross-validated data). Detailed diagnostic performance results are shown in Appendix E1 (online).

Discussion

The results of our study demonstrate that preoperative MR imaging values for pancreatic stiffness, MPD diameter, and stump area are highly significant determinants of POPF risk. Compared with palpatory assessment by the surgeon, MR elastography achieved better predictive power and accuracy for the prediction of both POPF and higher-grade POPF.

Consistent with previous studies (21,23,25,26), our univariate analysis showed that large body mass index, no history of weight loss, soft pancreas at palpation, nondilated MPD, large pancreas-to-duct ratio, large stump area and remnant volume, and extensively mobilized stump are all correlated with increased POPF risk. Furthermore, our multivariate analysis revealed that local differences in stump characteristics, both mechanical (lower pancreatic stiffness) and morphologic (MPD size and stump area), were independent risk factors for POPF. Softer pancreatic tissue combined with a nondilated MPD and a larger stump area creates a more challenging condition for suturing, which leads to a higher possibility of anastomotic fistula (21,23). The risk for POPF is minimized, regardless of any other risk factor, when the pancreatic stiffness is greater than1.59 kPa (1.51 kPa for high-grade POPF for 100% specificity). This is reasonable because a hard stump with advanced fibrosis and severe atrophy of the exocrine tissue permits easier anastomosis and secretes markedly less pancreatic juice. The detrimental effect of a larger stump area might be explained by greater suture requirements and more pancreatic juice, producing a higher likelihood of anastomosis leakage (21).

The lack of other significant factors in our multivariate analysis might be explained by their intrinsic correlation with stiffness or morphologic characteristics because these predictor variables are not independently associated with POPF risk. For instance, pancreatic texture by palpatory assessment was obviously correlated with MR elastography–determined stiffness. Similarly, pancreatic ductal adenocarcinoma and chronic pancreatitis are known to be associated with a dilated MPD and obstructive pancreatitis, and in our study they were correlated with MPD and pancreatic stiffness. Thus, preoperative MR evaluation, which reflects the morphologic and mechanical features of the stump, integrates the contribution of other risk factors into a single test, yielding a measurement that is more directly relevant to the POPF risk.

Imaging findings used to evaluate POPF risk primarily correspond to the degree of fibrosis in the stump (4,8). Diffusion-weighted–based techniques, imaging diffusion, and perfusion parameters have been used to assess fibrotic changes in tissue. However, in recent studies and in our study, ADCs have differed little among different fibrosis stages. Studies of intravoxel incoherent motion-derived quantitative parameters also had inconsistent results in terms of correlation with fibrotic progression (8,27) (ie, the perfusion fraction was negatively correlated with fibrosis in the study by Yoon et al [8] but had a trend toward positive correlation in the study by Hecht et al [27]). Of note, our study proved that MR elastography–based stiffness values were predominantly associated with pancreatic fibrosis, more strongly than were any other MR imaging parameter examined (28,29).

Morphologic measurements at the pancreatic stump are another set of independent predictors of POPF. These measurements were proved to be associated with the severity of acinar atrophy in our study, reflecting the proportion of viable acinar gland and, thus, the expected volume of pancreatic juice (21,24). Consistent with previous reports, MPD diameter and stump area were among the most reliable predictors of POPF.

Previous work has shown inconsistent relationships between fat infiltration and POPF risks. Although Lee et al (30) and Gaujoux et al (9) reported that fat infiltration contributed to higher POPF rates, it did not differ significantly among groups with different POPF grades in the study by Yoon et al (8) and our study. To our knowledge, our study was the first to identify a negative correlation between fat

Table 4: Diagnostic Performance of MR Elastography for Prediction of Postoperative Pancreatic Fistula and High-Grade (B and C) Postoperative Pancreatic Fistula: Raw Performance Parameters

	POPF		High-Grade POPF	
Parameter	Shear Stiffness	Palpation	Shear Stiffness	Palpation
Cutoff (kPa)	≤1.43	…	≤1.27	…
AUC*	0.78 (0.70, 0.87)	0.66 (0.57, 0.75)	0.82 (0.73, 0.91)	0.64 (0.53, 0.75)
Sensitivity (%)*	90.5 (77.4, 97.3) [38/42]	57.1 (41.0, 72.3) [24/42]	85.0 (62.1, 96.8) [17/20]	60.0 (36.1, 80.9) [12/20]
Specificity (%)*	58.6 (46.2, 70.2) [41/70]	67.1 (54.9, 77.9) [47/70]	72.8 (62.6, 81.6) [67/92]	62.0 (51.2, 71.9) [57/92]
PPV (%)	56.7 (44.0, 68.8) [38/67]	51.1 (36.1.0, 65.9) [24/47]	40.5 (25.6, 56.7) [17/42]	25.5 (13.9, 40.3) [12/47]
NPV (%)	91.1 (78.8, 97.5) [41/45]	72.3 (59.8, 82.7) [47/65]	95.7 (88.0, 99.1) [67/70]	87.7 (77.2, 94.5) [57/65]
Accuracy (%)*	70.5 (60.9, 77.4) [79/112]	63.4 (54.5, 72.3) [71/112]	73.2 (64.3, 81.3) [82/112]	61.6 (52.7, 70.5) [69/112]

Note.—Cutoff values were based on receiver operating characteristic curve analysis. Numbers in parentheses are 95% confidence intervals. Numbers in brackets are raw data. AUC = area under the receiver operating characteristic curve, NPV = negative predictive value, POPF = postoperative pancreatic fistula, PPV = positive predictive value.

* The area under the receiver operating characteristic curve for MR elastography was significantly higher than that of palpatory assessment for predicting both POPF risk ($P = .0006$) and high-grade POPF risk ($P = .003$). The McNemar test revealed that MR elastography had significantly higher sensitivity ($P < .001$) and accuracy ($P < .001$) than did palpation for predicting POPF risk and had significantly higher sensitivity ($P = .003$), specificity ($P = .03$), and accuracy ($P < .001$) for predicting high-grade POPF risk.

Table 5: Diagnostic Performance of MR Elastography for Prediction of Postoperative Pancreatic Fistula and High-Grade (B and C) Postoperative Pancreatic Fistula: Cross-Validated Performance Parameters

	POPF		High-Grade POPF	
Parameter	Shear Stiffness	Palpation	Shear Stiffness	Palpation
Cutoff (kPa)	≤1.43	…	≤1.27	…
AUC*	0.71 (0.63, 0.79)	0.62 (0.53, 0.72)	0.76 (0.66, 0.86)	0.61 (0.49, 0.73)
Sensitivity (%)*	83.3 (71.4, 92.9) [35/42]	57.1 (42.9, 71.4) [24/42]	80.0 (60.0, 95.0) [16/20]	60.0 (40.0, 80.0) [12/20]
Specificity (%)*	58.6 (47.1, 70.0) [41/70]	67.1 (55.7, 78.6) [47/70]	71.7 (62.0, 80.4) [66/92]	62.0 (52.2, 71.7) [57/92]
PPV (%)	54.7(47.1, 62.7) [35/64]	51.1 (40.5, 62.2) [24/47]	38.1 (29.3, 48.7) [16/42]	25.5 (17.1, 34.2) [12/47]
NPV (%)	85.4 (76.4, 93.8) [41/48]	72.3 (64.6, 80.3) [47/65]	94.3 (89.5, 98.6) [66/70]	87.7 (81.7, 93.8) [57/65]
Accuracy (%)*	67.9 (58.9, 75.9) [76/112]	63.4 (54.5, 72.3) [71/112]	73.2 (64.3, 81.3) [82/112]	61.6 (52.7, 70.5) [69/112]

Note.—Cutoff values were based on receiver operating curve analysis. Numbers in parentheses are 95% confidence intervals. Numbers in brackets are raw data. AUC = area under the receiver operating characteristic curve, NPV = negative predictive value, POPF = postoperative pancreatic fistula, PPV = positive predictive value.

* The area under the receiver operating characteristic curve for MR elastography was significantly higher than that of palpatory assessment for predicting both POPF risk ($P = .016$) and high-grade POPF risk ($P = .011$). The McNemar test revealed that MR elastography had higher sensitivity ($P = .003$) than palpation for predicting POPF risk and a trend toward higher accuracy without significance ($P = .383$). MR elastography also had significantly higher sensitivity ($P = .006$), specificity ($P = .05$), and accuracy ($P < .001$) for predicting high-grade POPF risk.

infiltration and MR elastography–determined pancreatic stiffness. The possible correlation of POPF risk and fatty pancreatic changes, observed by others, might be essentially due to an inherent relationship between soft texture and POPF risk. When fibrosis and acinar atrophy predominate to cause high stiffness (>1.59 kPa for POPF and 1.51 kPa for high-grade POPF), POPF risk was minimized regardless of lipomatosis. Therefore, we propose that these three stump-related MR parameters—lower pancreatic stiffness, nondilated MPD, and larger stump area (which indicate lower fibrosis, higher acinar excretion, and lipomatosis)—are highly predictive of higher POPF risk.

Our study has several limitations. First, this is a retrospective study; thus, additional, prospective, multicenter studies are required to independently validate these results. Second, MR elastography has lower resolution than does standard MR imaging pulse sequences. The recently proposed spin-echo echo-planar imaging MR elastography with three-dimensional processing can improve resolution and provide robust estimation of pancreatic stiffness (12,15,17). Third, most of our patients (86 of 112 patients) had a body mass index less than 25 kg/m^2, so our results should be confirmed in larger samples that include more overweight or obese patients. Fourth, our data were obtained from a single 3.0-T imager; therefore, data from 1.5-T units and different vendors should be analyzed in further studies. Fifth, we did not evaluate whether Dixon sequences and intravoxel incoherent motion-derived sequences helped predict POPF risk. Finally, the value of our reproducibility data is limited because reproducibility was based on only two readers.

In conclusion, quantitative preoperative MR assessments of mechanical and morphologic characteristics of the pancreatic stump are strongly predictive of pancreaticoenteric anastomotic fistula. Lower pancreatic stiffness was associated with relatively less pancreatic fibrosis, a higher grade of acinar atrophy, and lipomatosis. We believe that preoperative identification of patients at high risk for POPF will help improve overall care for patients undergoing pancreatectomy with pancreaticoenteric anastomosis.

Acknowledgment: We thank Jun Chen, PhD, from the Department of Radiology, Mayo Clinic, for his assistance with providing the tailored pancreatic MR elastography driver.

Author contributions: Guarantors of integrity of entire study, Y.S., Q.G.; study concepts/study design or data acquisition or data analysis/interpretation, all authors; manuscript drafting or manuscript revision for important intellectual content, all authors; approval of final version of submitted manuscript, all authors; agrees to ensure any questions related to the work are appropriately resolved, all authors; literature research, Y.S., Yangqing Liu, K.J.G., R.L.E., Q.G.; clinical studies, Y.S., Ying Liu, F.G., Yangqing Liu, Q.G.; statistical analysis, Y.S., R.L.E.; and manuscript editing, Y.S., S.T., Yue Li, K.J.G., R.L.E., Q.G.

Disclosures of Conflicts of Interest: **Y.S.** disclosed no relevant relationships. **Ying Liu** disclosed no relevant relationships. **F.G.** disclosed no relevant relationships. **Yanqing Liu** disclosed no relevant relationships. **S.T.** disclosed no relevant relationships. **Yue Li** disclosed no relevant relationships. **K.J.G.** Activities related to the present article: disclosed no relevant relationships. Activities not related to the present article: receives royalties from licensing of intellectual property related to MR elastography from Resoundant; institution receives royalties from licensing of intellectual property related to MR elastography from Resoundant; owns stock in Resoundant; institution owns stock in Resoundant. Other relationships: has a patent pending and a patent issued; has a patent licensed. **R.L.E.** Activities related to the present article: institution receives money for board membership at Resoundant; institution has grants/grants pending with Resoundant; institution has patents (planned, pending, or issued); shares royalties with institution; institution has stock/stock options in Resoundant; receives travel/accommodation/meeting expenses unrelated to activities listed from Resoundant. Activities not related to the present article: disclosed no relevant relationships. Other relationships: institution has patents pending, issued and licensed; institution receives royalties; receives a share of royalties from institution; has a patent licensed. **Q.G.** disclosed no relevant relationships.

References

1. Reid-Lombardo KM, Farnell MB, Crippa S, et al. Pancreatic anastomotic leakage after pancreaticoduodenectomy in 1,507 patients: a report from the Pancreatic Anastomotic Leak Study Group. J Gastrointest Surg 2007;11(11):1451–1458; discussion 1459.
2. Poon RT, Lo SH, Fong D, Fan ST, Wong J. Prevention of pancreatic anastomotic leakage after pancreaticoduodenectomy. Am J Surg 2002;183(1):42–52.
3. Tsiotos GG, Farnell MB, Sarr MG. Are the results of pancreatectomy for pancreatic cancer improving? World J Surg 1999;23(9):913–919.
4. Watanabe H, Kanematsu M, Tanaka K, et al. Fibrosis and postoperative fistula of the pancreas: correlation with MR imaging findings—preliminary results. Radiology 2014;270(3):791–799.
5. Tranchart H, Gaujoux S, Rebours V, et al. Preoperative CT scan helps to predict the occurrence of severe pancreatic fistula after pancreaticoduodenectomy. Ann Surg 2012;256(1):139–145.
6. Sugimoto M, Takahashi S, Kobayashi T, et al. Pancreatic perfusion data and post-pancreaticoduodenectomy outcomes. J Surg Res 2015;194(2):441–449.
7. Tajima Y, Kawabata Y, Hirahara N. Preoperative imaging evaluation of pancreatic pathologies for the objective prediction of pancreatic fistula after pancreaticoduodenectomy. Surg Today 2018;48(2):140–150.
8. Yoon JH, Lee JM, Lee KB, et al. Pancreatic steatosis and fibrosis: quantitative assessment with preoperative multiparametric MR imaging. Radiology 2016;279(1):140–150.
9. Gaujoux S, Cortes A, Couvelard A, et al. Fatty pancreas and increased body mass index are risk factors of pancreatic fistula after pancreaticoduodenectomy. Surgery 2010;148(1):15–23.
10. Pereira FL, Vasques FT, Moricz A, Campos T, Pacheco AM Jr, Silva RA. Correlation analysis between post-pancreatoduodenectomy pancreatic fistula and pancreatic histology. Rev Col Bras Cir 2012;39(1):41–47.
11. Shi Y, Xia F, Li QJ, et al. Magnetic resonance elastography for the evaluation of liver fibrosis in chronic hepatitis B and C by using both gradient-recalled echo and spin-echo echo planar imaging: a prospective study. Am J Gastroenterol 2016;111(6):823–833.
12. Shi Y, Glaser KJ, Venkatesh SK, Ben-Abraham EI, Ehman RL. Feasibility of using 3D MR elastography to determine pancreatic stiffness in healthy volunteers. J Magn Reson Imaging 2015;41(2):369–375.
13. Yin Z, Magin RL, Klatt D. Simultaneous MR elastography and diffusion acquisitions: diffusion-MRE (dMRE). Magn Reson Med 2014;71(5):1682–1688.
14. Mariappan YK, Glaser KJ, Levin DL, et al. Estimation of the absolute shear stiffness of human lung parenchyma using (1) H spin echo, echo planar MR elastography. J Magn Reson Imaging 2014;40(5):1230–1237.
15. An H, Shi Y, Guo Q, Liu Y. Test-retest reliability of 3D EPI MR elastography of the pancreas. Clin Radiol 2016;71(10):1068.e7–1068.e12.
16. Glaser KJ, Manduca A, Ehman RL. Review of MR elastography applications and recent developments. J Magn Reson Imaging 2012;36(4):757–774.
17. Shi Y, Gao F, Li Y, et al. Differentiation of benign and malignant solid pancreatic masses using magnetic resonance elastography with spin-echo echo planar imaging and three-dimensional inversion reconstruction: a prospective study. Eur Radiol 2018;28(3):936–945.
18. Manduca A, Lake DS, Kruse SA, Ehman RL. Spatio-temporal directional filtering for improved inversion of MR elastography images. Med Image Anal 2003;7(4):465–473.
19. Kawai M, Hirono S, Okada K, et al. Randomized controlled trial of pancreaticojejunostomy versus stapler closure of the pancreatic stump during distal pancreatectomy to reduce pancreatic fistula. Ann Surg 2016;264(1):180–187.
20. Arai T, Kobayashi A, Yokoyama T, et al. Signal intensity of the pancreas on magnetic resonance imaging: prediction of postoperative pancreatic fistula after a distal pancreatectomy using a triple-row stapler. Pancreatology 2015;15(4):380–386.
21. Ridolfi C, Angiolini MR, Gavazzi F, et al. Morphohistological features of pancreatic stump are the main determinant of pancreatic fistula after pancreatoduodenectomy. BioMed Res Int 2014;2014:641239.
22. Bassi C, Dervenis C, Butturini G, et al. Postoperative pancreatic fistula: an international study group (ISGPF) definition. Surgery 2005;138(1):8–13.
23. Wellner UF, Kayser G, Lapshyn H, et al. A simple scoring system based on clinical factors related to pancreatic texture predicts postoperative pancreatic fistula preoperatively. HPB 2010;12(10):696–702.
24. Hatano M, Watanabe J, Kushihata F, et al. Quantification of pancreatic stiffness on intraoperative ultrasound elastography and evaluation of its relationship with postoperative pancreatic fistula. Int Surg 2015;100(3):497–502.
25. Sugimoto M, Takahashi S, Kojima M, et al. What is the nature of pancreatic consistency? Assessment of the elastic modulus of the pancreas and comparison with tactile sensation, histology, and occurrence of postoperative pancreatic fistula after pancreaticoduodenectomy. Surgery 2014;156(5):1204–1211.
26. Tajima Y, Kuroki T, Tsutsumi R, et al. Risk factors for pancreatic anastomotic leakage: the significance of preoperative dynamic magnetic resonance imaging of the pancreas as a predictor of leakage. J Am Coll Surg 2006;202(5):723–731.
27. Hecht EM, Liu MZ, Prince MR, et al. Can diffusion-weighted imaging serve as a biomarker of fibrosis in pancreatic adenocarcinoma? J Magn Reson Imaging 2017;46(2):393–402.
28. Ichikawa S, Motosugi U, Morisaka H, et al. MRI-based staging of hepatic fibrosis: comparison of intravoxel incoherent motion diffusion-weighted imaging with magnetic resonance elastography. J Magn Reson Imaging 2015;42(1):204–210.
29. Wang QB, Zhu H, Liu HL, Zhang B. Performance of magnetic resonance elastography and diffusion-weighted imaging for the staging of hepatic fibrosis: a meta-analysis. Hepatology 2012;56(1):239–247.
30. Lee SE, Jang JY, Lim CS, et al. Measurement of pancreatic fat by magnetic resonance imaging: predicting the occurrence of pancreatic fistula after pancreatoduodenectomy. Ann Surg 2010;251(5):932–936.